

# Static and dynamical properties of a hard-disk fluid confined to a narrow channel

M. J. Godfrey and M. A. Moore

*School of Physics and Astronomy, University of Manchester, Manchester M13 9PL, UK*

(Dated: September 24, 2018)

The thermodynamic properties of disks moving in a channel sufficiently narrow that they can collide only with their nearest neighbors can be solved exactly by determining the eigenvalues and eigenfunctions of an integral equation. Using it we have determined the correlation length  $\xi$  of this system. We have developed an approximate solution which becomes exact in the high density limit. It describes the system in terms of defects in the regular zigzag arrangement of disks found in the high-density limit. The correlation length is then effectively the spacing between the defects. The time scales for defect creation and annihilation are determined with the help of transition-state theory, as is the diffusion coefficient of the defects, and these results are found to be in good agreement with molecular dynamics simulations. On compressing the system with the Lubachevsky–Stillinger procedure, jammed states are obtained whose packing fractions  $\phi_J$  are a function of the compression rate  $\gamma$ . We find a quantitative explanation of this dependence by making use of the Kibble–Zurek hypothesis. We have also determined the point-to-set length scale  $\xi_{PS}$  for this system. At a packing fraction  $\phi$  close to its largest value  $\phi_{\max}$ ,  $\xi_{PS}$  has a simple power law divergence,  $\xi_{PS} \sim 1/(1 - \phi/\phi_{\max})$ , while  $\xi$  diverges much faster,  $\ln(\xi) \sim 1/(1 - \phi/\phi_{\max})$ .

## I. INTRODUCTION

Glasses and supercooled liquids have attracted a great deal of attention from both experimentalists and simulators, but despite this no totally satisfactory description of them is available. There is a suggestion that there is a connection between glassy behavior and jammed states [1]. In this paper we shall examine a model – a system of hard disks confined to move in a narrow channel – which is sufficiently simple that we can calculate analytically quantities which in two and three dimensional systems have not yet been satisfactorily studied despite extensive numerical efforts. Bowles and colleagues [2–4] have studied this model primarily by numerical methods and have elucidated many of its features, including the numbers and properties of the jammed states and the dynamics of the fluid states. In this paper, we continue their studies but our approach is primarily analytic. This has the advantage of providing physical insights as to what is going on.

The model consists of  $N$  disks of diameter  $\sigma$ , which move in a narrow channel consisting of two impenetrable walls (lines) spaced by a distance  $H_d$  such that  $1 < H_d/\sigma < 1 + \sqrt{3}/4$  (see Fig. 1). The upper limit is imposed so that only nearest-neighbor disk interactions can arise; also the disks cannot pass each other, so their initial ordering is preserved for all times. The disks and the walls are hard, so that configurations of the disks where the centers approach by a distance less than  $\sigma$  cannot occur, and the center of each disk must be at a distance of at least  $\sigma/2$  from each wall. It is useful to introduce the following notation, which is also illustrated in Fig. 1. Let the Cartesian coordinates of the center of disk  $i$  be denoted by  $(x_i, y_i)$ , where the  $x$ -axis coincides with the center-line of the channel. A *configuration* is a set of disk positions  $(x_i, y_i)$ ,  $i = 1, \dots, N$ , that is consistent with the constraints of no overlap. Let  $h = H_d - \sigma$ . Then, because of the hard walls, the allowed range of  $y_i$  is

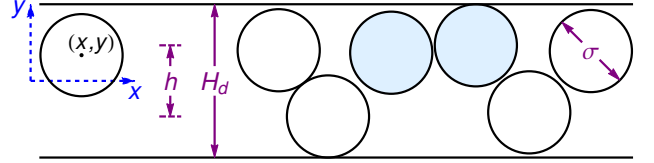


FIG. 1: (Color online) Geometry of the disks in a narrow channel. The disks are of diameter  $\sigma$  and the channel is of width  $H_d$ .  $h = H_d - \sigma$  is the width of the channel which is available to the centers of the disks. The coordinates of the center of  $i$ th disk are  $(x_i, y_i)$ , where  $y_i$  is measured from the centerline of the channel. The blue-shaded disks are a defect in the zigzag arrangement of the disks that is favored at high density.

$-h/2 \leq y_i \leq h/2$ . The packing fraction or occupied volume is  $\phi = N\pi\sigma^2/(4LH_d)$ , where  $L$  is the length of the channel along the  $x$ -direction. The maximum possible value of  $\phi$  will be called  $\phi_{\max}$ . It is given by

$$\phi_{\max} = \frac{\pi\sigma^2}{4H_d\sqrt{\sigma^2 - h^2}}. \quad (1)$$

The numerical work described in this paper has been done for the case when  $h = \sqrt{3}/4\sigma$ , for which  $\phi_{\max} \simeq 0.8418$ . A possible configuration of the disks is shown in Fig. 1, while the configuration associated with the maximum possible packing fraction,  $\phi_{\max}$ , is the zigzag configuration shown in Fig. 9(a). Note that when  $h = \sqrt{3}/4\sigma$ , the centers of the disks form a regular array of equilateral triangles in this, the most densely packed state.

In Sec. II we describe the transfer matrix formalism that enables us to calculate exactly the equilibrium static properties from the eigenvalues and eigenfunctions of an integral equation. One can determine the equation of state of the system from the largest eigenvalue and its

associated eigenfunction, and the correlation length  $\xi$  of the system is given by the logarithm of the ratio of the largest and next-largest eigenvalues. The transfer matrix formalism gives few insights as to what is going on, so in Sec. III we discuss an analytical approximation which becomes exact in the high density limit  $\phi \rightarrow \phi_{\max}$ . This leads us to understand the nature of the order that is growing in the system at high density. This order is the zigzag arrangement of the disks, which, for  $\phi < \phi_{\max}$ , can be interrupted by defects, like the blue-shaded disks in Fig. 1 and also in Figs. 7 and 9. It is shown that the correlation length  $\xi$  is a measure of the distance between the defects. We shall calculate  $\theta$ , which is the average concentration of defects, as a function of the packing fraction  $\phi$ .

In Ref. [4] it was found that, just as for two- and three-dimensional hard sphere systems, there is a packing fraction  $\phi_d$  above which the dynamics becomes activated, and the activated dynamics was studied as a function of the packing fraction  $\phi$ . In Sec. IV we shall show that this dynamics can be understood analytically in the limit  $\phi \rightarrow \phi_{\max}$ . The same approximation is fairly good over the entire range of  $\phi$  between  $\phi_d$  and  $\phi_{\max}$ . The correlation length  $\xi$  grows rapidly for  $\phi < \phi_d$  but does not diverge at  $\phi_d$ . We are able to make analytical progress using the transition-state approximation for those aspects of the dynamics associated with the creation and annihilation of defects and their diffusion. The configurational entropy associated with the jammed states has been calculated analytically [3] and the same authors have used the Lubachevsky–Stillinger algorithm [5] to determine how  $\phi_J$ , the packing fraction at jamming, depends on the compression rate. In this paper we shall show that this dependence can be modeled by using the Kibble–Zurek [6, 7] hypothesis.

In Sec. V we calculate the point-to-set length  $\xi_{PS}$ . It is much smaller than  $\xi$  and has a quite different dependence on  $\phi$ . This might suggest that not all length scales in glasses are fundamentally equivalent when they become large, but we also point out that our system has some properties (most notably a growing crystalline order) which are thought not to be of importance in three dimensional glasses.

## II. EQUILIBRIUM PROPERTIES VIA THE TRANSFER MATRIX

In this section we set up the formalism by which the equation of state and correlation length  $\xi$  can be obtained, at least numerically, from study of an integral equation. We follow the procedure used in Ref. [8]. The canonical partition function is

$$\exp(-\beta A_L) = \frac{1}{\Lambda^{2N}} \prod_{i=1}^N \int dx_i \int_{-h/2}^{h/2} dy_i I, \quad (2)$$

where  $(x_i, y_i)$  are the coordinates of the disk centers, with the ordering  $0 < x_1 < \dots < x_N < L$ , where  $L$  is the

length of the channel available to the disk centers. The integrand  $I$  is 1 if the configuration of  $(x_i, y_i)$  is allowed but is zero if any two disks overlap.  $d$  is the dimensionality of the channel, i.e.  $d = 2$ .  $\Lambda = (2\pi\beta\hbar^2/m)^{1/2}$  is the thermal wavelength. For given values of the coordinates  $y_i$  the system is isomorphic to a mixture of one-dimensional hard rods of various lengths which allows the integrations over the  $x_i$  to be performed [9]. Then

$$\exp(-\beta A_L) = \frac{1}{\Lambda^{2N} N!} \prod_{i=1}^N \int_{-h/2}^{h/2} dy_i [L - \sum_{j=1}^{N-1} \sigma(y_j, y_{j+1})]^N I',$$

where  $\sigma(y_i, y_{i+1})$  is the distance of closest approach of neighboring disks  $i$  and  $i+1$  in the direction along the axis, i.e.  $[\sigma^2 - (y_i - y_{i+1})^2]^{1/2}$ . The sum  $\sum_{j=1}^{N-1} \sigma(y_j, y_{j+1})$  is the total excluded volume of the “hard rods”, which must be smaller than  $L$ ; this constraint is imposed by the integrand  $I'$ , which can be either 0 or 1.

It is convenient to perform a Legendre transform of the Helmholtz free energy  $A_L$  by calculating the partition function

$$\exp(-\beta\Phi) = \beta f \int_0^\infty dL \exp(-\beta A_L) \exp(-\beta f L), \quad (3)$$

where  $f$  can be regarded as the force exerted by a piston at the end of the channel; the longitudinal pressure  $P$  is given by  $P = f/h$ , as  $h$  is the width of the channel accessible to the particle centers. A prefactor  $\beta f$  has been introduced in (3) to ensure dimensional homogeneity; it is irrelevant to the thermodynamics. The integral over  $L$  can now be performed, giving

$$\exp(-\beta\Phi) = \frac{1}{(\beta f \Lambda^2)^N} \times \prod_{i=1}^N \int_{-h/2}^{h/2} dy_i e^{-\beta f \sum_{j=1}^{N-1} \sigma(y_j, y_{j+1})}. \quad (4)$$

The calculation of the potential  $\Phi$  now manifestly involves only nearest-neighbor interactions. When  $N$  is large,  $\Phi$  is given by [8]

$$\beta\Phi \simeq N \ln(\beta f \Lambda^2 / \lambda_1), \quad (5)$$

where  $\lambda_1$  (with the dimensions of length) is the largest eigenvalue of the integral equation

$$\lambda_n u_n(y_1) = \int_{-h/2}^{h/2} e^{-\beta f \sigma(y_1, y)} u_n(y) dy. \quad (6)$$

Equation (6) can be solved numerically by approximating the integral by a sum, which leads to a symmetric matrix eigenvalue problem [8]. When  $\beta f \sigma$  is large, most of the variation in the functions  $u_n$  is concentrated near the walls of the channel, so that it is helpful to make a transformation of the variable  $y$  before discretizing [10].

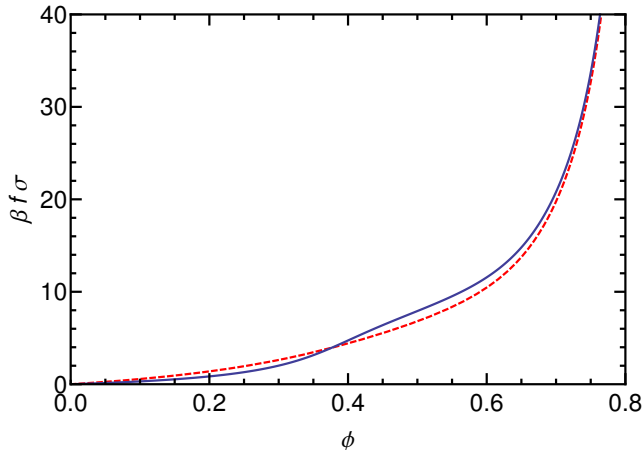


FIG. 2: (Color online) The equation of state of the narrow-channel system; that is,  $\beta f \sigma$  versus the packing fraction  $\phi$ . The solid line results are from the transfer matrix and are essentially exact. Also shown (red dashed line) are the results from our analytical approximation Eqs. (18, 20). Note that at large  $\phi$  there is excellent agreement between the two.

All of the equilibrium properties of the system can, in principle, be determined from the eigenvalues and eigenfunctions of (6). For example, the equation of state, i.e. the relation between  $f$  and the packing fraction  $\phi$ , can be found from [8]

$$L/N = \frac{1}{\beta f} + \frac{1}{\lambda_1} \int_{-h/2}^{h/2} \int_{-h/2}^{h/2} u_1(y_1) u_1(y_2) \times \sigma(y_1, y_2) e^{-\beta f \sigma(y_1, y_2)} dy_1 dy_2, \quad (7)$$

which avoids the numerical differentiation that would be required to calculate  $L$  directly from  $L = \partial \Phi / \partial f$ .

The plot of  $\beta f \sigma$  versus  $\phi$  is shown in Fig. 2. We suspect that the “shoulder” that appears near  $\phi \simeq 0.5$  could be the remnant of the first order transition which is seen in genuine two-dimensional systems [11]. The pressure (or force) goes to infinity as the density of the system approaches  $\phi_{\max}$ . The form of this divergence will be discussed in Sec. III.

The logarithm of the ratio of the two largest eigenvalues of the integral equation gives a correlation length  $\xi$ , which is plotted in Fig. 3. The meaning of  $\xi$  is that it is the number of disks that typically form the zigzag pattern seen in the defect-free regions of Fig. 1. More precisely, it measures the decay of the correlation between the  $y$ -coordinates of well-separated disks  $i$  and  $i + s$ ,

$$|\langle y_i y_{i+s} \rangle| \sim \exp(-s/\xi), \quad (8)$$

where  $s \gg 1$ . Notice that  $\xi$  is dimensionless, because  $s$  is an integer; of course, if one knows the packing fraction, one can convert  $\xi$  into a distance by multiplying by the

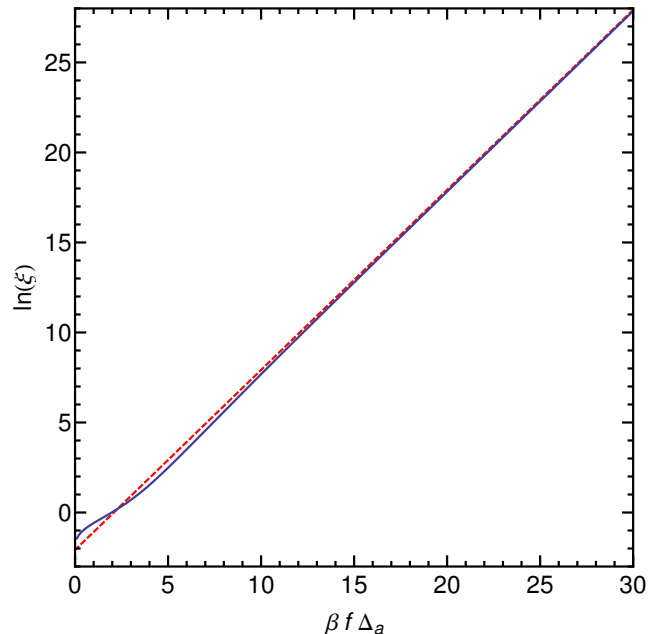


FIG. 3: (Color online) The logarithm of the correlation length  $\ln(\xi)$  versus  $\beta f \Delta_a$  obtained from the transfer matrix (full line).  $\Delta_a$  is the extra length associated with a defect, which is discussed in Sec. III at Eq. (22). It is given by  $\Delta_a = \sigma - \sqrt{\sigma^2 - h^2}$ . The red dashed line is the prediction of our analytical work, Eq. (26).

average separation of neighboring disks. Fig. 3 shows that as  $\phi \rightarrow \phi_{\max}$ ,  $\xi$  grows rapidly, reflecting the fact that  $\xi$  is essentially the spacing between the defects, which becomes very large in this limit. This observation will be made quantitative in Sec. III.

The behavior of  $\xi$  at smaller packing fractions is also of interest. In Fig. 4 we have plotted the reciprocal of  $\xi$  versus the packing fraction. The fitted straight line extrapolates to a value  $\phi_d \simeq 0.48$ . This packing fraction was identified in Ref. [4] as the density above which the dynamics becomes activated (see Fig. 8). Similar behavior arises for hard spheres in three dimensions at  $\phi = \phi_d \simeq 0.58$  and is attributed there to the onset of caging. In the mode-coupling approximation this is accompanied by a diverging length scale, but in a better approximation this length scale would be expected to remain finite [12]. The same features seem to be present in this system of disks in a channel. The data in Fig. 4 shows that between  $\phi = 0.1$  up to  $\phi = 0.4$  the growth of  $\xi$  is approximated well by

$$\xi \sim \frac{a}{1 - \phi/\phi_d}. \quad (9)$$

Fig. 4 shows that there is not a true divergence of  $\xi$  at  $\phi_d$ : the apparent divergence is rounded off and at  $\phi = \phi_d$ ,  $\xi$  is approximately 4. This just means that at this density the

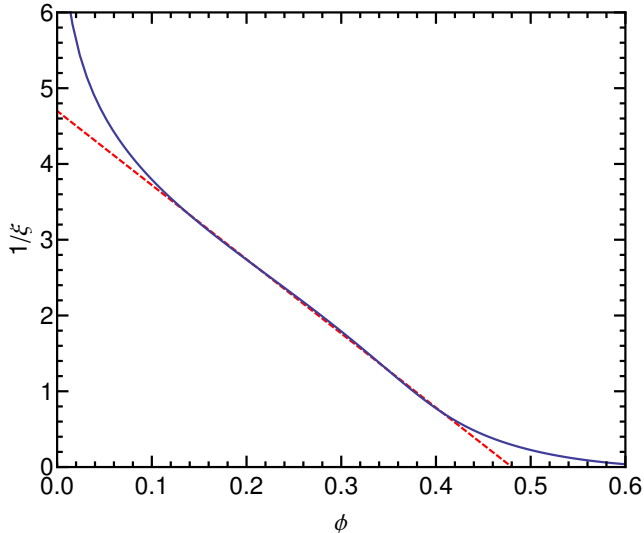


FIG. 4: (Color online) The reciprocal correlation length  $1/\xi$  versus the packing fraction  $\phi$  (blue solid curve). The red dashed line is a straight-line fit to highlight the rapid growth of  $\xi$  as  $\phi \rightarrow \phi_d \simeq 0.48$ . There is no true divergence of  $\xi$  at the dynamical transition packing fraction  $\phi_d$  and the “transition” is rounded-off.

growth of zigzag order has grown to involve four adjacent disks, so that the disks will typically no longer be able to bounce from one wall to another unless they first push other disks away. In other words, above  $\phi_d$  the disks are caged. Escape from the cage requires the collective motion of several disks, a process which will be studied in more detail in Sec. IV. We believe also that the onset of caging behavior is also ultimately responsible for the strong fluid to fragile fluid crossover behavior described in Ref. [2]. For  $\phi > \phi_d$  the dynamics is fragile, as the caging causes relaxation times to increase faster than would be expected on a simple Arrhenius picture.

If the analogy with hard spheres near  $\phi_d \simeq 0.58$  is appropriate then a suitable autocorrelation function for studying glassy behavior in our system would seem to be

$$A(t) = \frac{\langle y_i(0)y_i(t) \rangle}{\langle y_i^2 \rangle}. \quad (10)$$

$A(t)$  will equal unity at  $t = 0$  and, as  $\phi \rightarrow \phi_d$ , one would expect a plateau to develop for larger times. After a time  $\tau_\alpha$ , the “alpha” relaxation time,  $A(t)$  starts to decay to zero as the disks escape their cages and  $\langle y_i(t) \rangle$  approaches zero. The study of this autocorrelation function will be published separately [13].

Several groups have extracted a dynamical length scale from the four point dynamical susceptibility of bulk colloidal matter, or via simulations of it for hard spheres and disks [14–16]. In these studies the length scale relates to the average number of particles that are cooperating in a

dynamic heterogeneous event. We suspect that this dynamical length therefore might relate to our length scale  $\xi$ , which is also a measure of the number of particles which move cooperatively, but see Ref. [12].

### III. RESULTS FOR LARGE DENSITIES

Using the integral equation (6) to solve for the equilibrium properties gives little insight as to what is going on, and it becomes increasingly difficult as  $\phi \rightarrow \phi_{\max}$ . Analytical progress is, however, possible in that limit, because every disk is typically found within a small distance of order  $1/(\beta f)$  from a wall. The disks form the zigzag pattern shown in Fig. 1 with relatively few defects, where a defect is a pair of disks (like those shaded in Fig. 1) that lie close to the same wall of the channel. We begin by calculating  $\theta$ , the concentration of these defects present in the system at equilibrium.

When  $\beta f$  is large, the largest contributions to the partition function (4) come from the neighborhoods of jammed states in which every disk is in contact with its two neighbors and a wall of the channel. Each jammed state is a local minimum of the excluded volume  $\sum_j \sigma(y_j, y_{j+1})$ , which is the reason its neighborhood makes a relatively large contribution to the partition function. We calculate these contributions below.

It is convenient to introduce new integration variables to parametrize a configuration in the neighborhood a jammed state. We define  $z_i$  to be the distance of disk  $i$  from its confining wall at  $y = \pm h/2$ .

For neighboring disks 1 and 2 on opposite sides of the channel, the contribution to the excluded volume is

$$\begin{aligned} \sigma(1, 2) &= \sqrt{\sigma^2 - (h - z_1 - z_2)^2} \\ &\simeq \sqrt{\sigma^2 - h^2} + \frac{h}{\sqrt{\sigma^2 - h^2}}(z_1 + z_2). \end{aligned} \quad (11)$$

Neighboring disks on the same side of the channel make a contribution  $\sigma(1, 2) \simeq \sigma + O[(z_1 - z_2)^2/\sigma]$ ; in this case, there is no term linear in  $z_1$  or  $z_2$ .

The jammed states can be more fully specified by stating the number and arrangement of defects within them. We suppose that there are  $M$  defects in a particular jammed state. Any one of the disks in this state will either have both of its neighbors on the opposite side of the channel if it forms part of the zigzag pattern, or it will have one neighbor on the same side of the channel and the other on the opposite side if it is part of a defect. (Configurations in which three or more disks lie adjacent at the same wall need not be considered, as they are unstable under compression: there is no barrier to moving the central disk to the opposite side of the channel.) We can renumber the disks  $k = 1$  to  $2M$  for those belonging to defect pairs and  $k = 2M + 1$  to  $N$  for those which do not. With this renumbering, and in terms of the new

variables  $z_k$ , the excluded volume can be written

$$\sum_{i=1}^{N-1} \sigma(y_i, y_{i+1}) \simeq (N-M)\sqrt{\sigma^2 - h^2} + M\sigma + \sum_{k=1}^{2M} \frac{hz_k}{\sqrt{\sigma^2 - h^2}} + \sum_{k=2M+1}^N \frac{2hz_k}{\sqrt{\sigma^2 - h^2}}, \quad (12)$$

to first order in the variables  $z_k$ . We insert this expression into Eq. (4) and integrate from  $z_k = 0$  to  $\infty$ ; formally,  $z_k$  should always be smaller than  $h$ , but when  $\beta f$  is large the error due to extending the range of integration is exponentially small. The resulting contribution to (4) is

$$\frac{1}{(\beta f \Lambda^2)^N} \left( \frac{\sqrt{\sigma^2 - h^2}}{\beta f h} \right)^{2M} \left( \frac{\sqrt{\sigma^2 - h^2}}{2\beta f h} \right)^{N-2M} e^{-\beta f [(N-M)\sqrt{\sigma^2 - h^2} + M\sigma]}, \quad (13)$$

which depends only on  $M$ , and not on the detailed arrangement of the defects. To obtain the total contribution from all states with  $M$  defects, we must multiply (13) by the number of these arrangements, which is approximately

$$W_M = \frac{(N-M)!}{M!(N-2M)!}. \quad (14)$$

The combinatoric factor  $W_M$  has a simple explanation. Each of the  $M$  defects consists of a pair of neighboring disks. This accounts for  $2M$  disks; the remaining  $N - 2M$  “free” disks are not part of any defect. The defect configurations can be regarded as arrangements of  $M$  defect-pairs and  $N - 2M$  free disks, in which adjacent *objects* (defect-pairs or free disks) occur alternately on opposite sides of the channel. The number of arrangements of  $N - M$  objects,  $M$  of one kind and  $N - 2M$  of another, is the factor  $W_M$  given in Eq. (14).

[The preceding argument for  $W_M$  ignores the facts that, in a rectangular channel, the first and last disks must, for stability, be *free* disks, and that, for any given  $M$ , there are two possible arrangements for this pair. The remaining  $N - 2 - 2M$  free disks and  $M$  defect-pairs can be permuted arbitrarily, which leads to  $2 \times (N - 2 - M)! / [(N - 2 - 2M)! M!]$  as the correct combinatoric factor. The difference compared with (14) is unimportant in the application below, in which we use the thermodynamic limit of  $\ln W_M$ . It may be noted that we have also ignored the special nature of the first and last disks in the right-hand side of Eq. (12). Treating these correctly would change the exponents in (13) by  $\pm 2$ , which again is unimportant in the thermodynamic limit.]

After combining the results of Eqs. (13) and (14) we find

$$\exp(-\beta\Phi) = \frac{1}{(\beta f \Lambda^2)^N} \sum_M W_M e^{-\beta f [(N-M)\sqrt{\sigma^2 - h^2} + M\sigma]} \left( \frac{\sqrt{\sigma^2 - h^2}}{\beta f h} \right)^N \frac{1}{2^{N-2M}}. \quad (15)$$

In the thermodynamic limit we can convert the sum over  $M$  to an integral over  $\theta$ , where  $M = \theta N$ , and write

$$\exp(-\beta\Phi) = N \int d\theta \exp[-\beta\Phi^*(N, \beta f, \theta)]. \quad (16)$$

The effective free energy  $\Phi^*$  is given by

$$\beta\Phi^*(N, \beta f, \theta) = -N \left\{ (1-\theta) \ln(1-\theta) - \theta \ln \theta - (1-2\theta) \ln(1-2\theta) - \beta f [(1-\theta)\sqrt{\sigma^2 - h^2} + \theta\sigma] + \ln \frac{\sqrt{\sigma^2 - h^2}}{h} - 2 \ln(\beta f \Lambda) - (1-2\theta) \ln 2 \right\}, \quad (17)$$

in which we have used Stirling’s approximation for the

logarithms of factorials. For large  $N$  the integral in

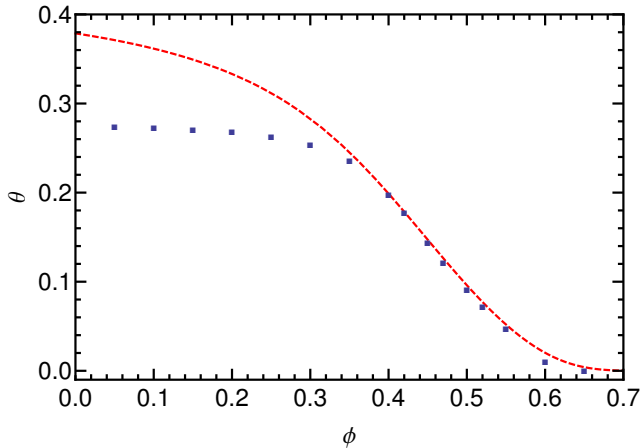


FIG. 5: (Color online) Plot of  $\theta = \langle M \rangle / N$ , the average density of defects, against  $\phi$ . The data points are from the simulations in [4], while the (red) dashed line is from solving Eqs. (18) and (20). This analytical solution is expected to be an increasingly good approximation as  $\phi$  approaches  $\phi_{\max}$ .

Eq. (16) can be done by steepest descents by finding the solution of  $\partial\Phi^*(N, \beta f, \theta)/\partial\theta = 0$ . This yields an equation for the equilibrium value of the defect density  $\theta$ ,

$$\frac{\theta(1-\theta)}{(1-2\theta)^2} = 4 \exp[\beta f(\sqrt{\sigma^2 - h^2} - \sigma)]. \quad (18)$$

From the relation  $L = \partial\Phi^*/\partial f$  we can obtain the equilibrium length of the system,

$$L = N[(1-\theta)\sqrt{\sigma^2 - h^2} + \theta\sigma] + \frac{2N}{\beta f}. \quad (19)$$

This can be rearranged to give the approximate equation of state

$$\beta f = \frac{2N}{L - N[(1-\theta)\sqrt{\sigma^2 - h^2} + \theta\sigma]}. \quad (20)$$

From Eqs. (18, 20) we can calculate  $\beta f\sigma$  and  $\theta$  in terms of  $\phi$ , as shown in Figs. 2 and 5. In the high density limit, the agreement is excellent as would be expected, but what is more surprising is that the agreement is fairly good down to quite low values of the packing fraction,  $\phi \simeq \phi_d$ .

In the limit when  $\beta f\sigma$  is large,  $\theta$  is small, and Eq. (18) simplifies to

$$\theta \simeq 4 \exp[-\beta f(\sigma - \sqrt{\sigma^2 - h^2})]. \quad (21)$$

The exponential can be understood as an ordinary Boltzmann factor. The extra length  $\Delta_a$  involved in inserting a single defect into the system over the length in the state of maximum density is

$$\Delta_a = \sigma - \sqrt{\sigma^2 - h^2}. \quad (22)$$

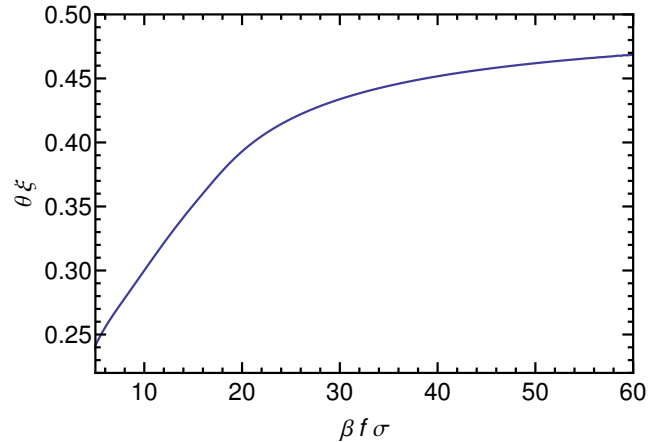


FIG. 6: (Color online)  $\theta\xi$  versus  $\beta f\sigma$ . Here  $\theta$  was obtained from the solution of Eqs. (18, 20) and  $\xi$  from the transfer-matrix solution. As  $\beta f\sigma$  becomes large, Eq. (25) predicts that  $\theta\xi \rightarrow 1/2$ .

The work done increasing the length against the applied force is  $\Delta E = f\Delta_a$ , so the exponential in Eq. (21) is just the usual Boltzmann expression  $\exp(-\beta\Delta E)$ .

The equation of state, Eq. (20), can be simplified in the limit of large  $\beta f\sigma$ , when  $\theta \rightarrow 0$ , giving

$$\beta f \simeq \frac{2N}{L(1 - \phi/\phi_{\max})}, \quad (23)$$

which is consistent with the general results of Salsburg and Wood [17] for the limit  $\phi \rightarrow \phi_{\max}$ .

Intuitively, one would expect there to be a relation between the density of defects  $\theta$  and the correlation length  $\xi$ , with  $\theta \sim 1/\xi$ : the correlation length should be comparable with the spacing between the defects. Fig. 6 bears this out and further suggests that as  $\phi \rightarrow \phi_{\max}$  the product  $\theta\xi \rightarrow 1/2$ . This result can be understood as follows. In the limit  $\phi \rightarrow \phi_{\max}$ , the defects are very dilute and are almost independent of one another. The probability  $P_k(r)$  that there will be  $k$  defects between disks  $i$  and  $i+r$  should therefore follow a Poisson distribution,

$$P_k(r) = \frac{1}{k!}(\theta r)^k \exp(-\theta r). \quad (24)$$

In the high-density limit, the disks are pressed tightly against the walls, so each  $y_i$  is approximately  $\pm h/2$ . The probability that  $y_i y_{i+r} \simeq +(h/2)^2$  is then the probability that there is an even number of defects between  $i$  and  $i+r$ , which is equal to the sum

$$P_{\text{even}} = \sum_{k=0}^{\infty} P_{2k}(r) = [1 + e^{-2\theta r}]/2,$$

while the probability that  $y_i y_{i+r} \simeq -(h/2)^2$  is the probability that there is an odd number of defects between  $i$

and  $i + r$ , which is the sum

$$P_{\text{odd}} = \sum_{k=0}^{\infty} P_{2k+1}(r) = [1 - e^{-2\theta r}]/2.$$

From these,

$$\begin{aligned} \langle y_i y_{i+r} \rangle &\simeq (h/2)^2 (P_{\text{even}} + (-1)P_{\text{odd}}) \\ &= (h/2)^2 \exp(-2\theta r) \\ &\equiv (h/2)^2 \exp(-r/\xi). \end{aligned} \quad (25)$$

Thus  $2\theta = 1/\xi$ , or  $\theta\xi = 1/2$  at high density. The form of  $\xi$  as  $\phi \rightarrow \phi_{\text{max}}$  is therefore

$$\xi \simeq \frac{1}{8} \exp(\beta f \Delta_a). \quad (26)$$

This result is clearly consistent with the numerical results shown in Fig. 3. The argument of the exponential can also be understood by calculating the defect free energy  $\delta F \simeq f\Delta_a - k_B T \ln \xi$ . The first term is the energy cost of creating the defect; the second is the reduction in its free energy by the entropy of placing it at any of  $\xi$  positions. Equating the defect free energy to zero gives the exponential in Eq. (26).

While the system of disks in a narrow channel has been studied for the insight it could provide on glass behavior in three dimensions, there is one striking difference between it and typical three dimensional glasses. It is that we *understand* the origin in the narrow channel system of its growing static length scale  $\xi$ : it quantifies the growth of the zigzag order as  $\phi \rightarrow \phi_{\text{max}}$ . This growth would also be expected to be visible in the structure factor  $S(q_x, q_y)$  as Bragg-like peaks at the wavevectors corresponding to that of the zigzag pattern (i.e., multiples of  $q_x = 2\pi/\sqrt{\sigma^2 - h^2}$  and  $q_y = 2\pi/h$ ) which would grow as  $\phi \rightarrow \phi_{\text{max}}$ . This feature of the narrow-channel system reflects the fact that the most dense state has crystalline order, and at lower densities the growing length scale  $\xi$  is a measure of the extent of the short-range crystalline order. The crystalline order is broken by the (topological!) defects and the correlation length  $\xi$  is basically the spacing between the defects. In three dimensions it is found that the structure factor hardly alters at densities close to  $\phi_d$ , but it is sometimes suggested that glass behavior might be associated with changes in more subtle correlations; see e.g. [18, 19]. We suspect that higher correlation functions will describe the onset of caging and must therefore contain a growing length scale. But these correlation functions have yet to be identified, and they may turn out to depend on the details of the intermolecular potential.

#### IV. DYNAMICS

Glass behavior is largely a dynamic phenomenon and in this section we shall analyse a few aspects of the dynamics of our system which are sufficiently simple to permit an analytical treatment.

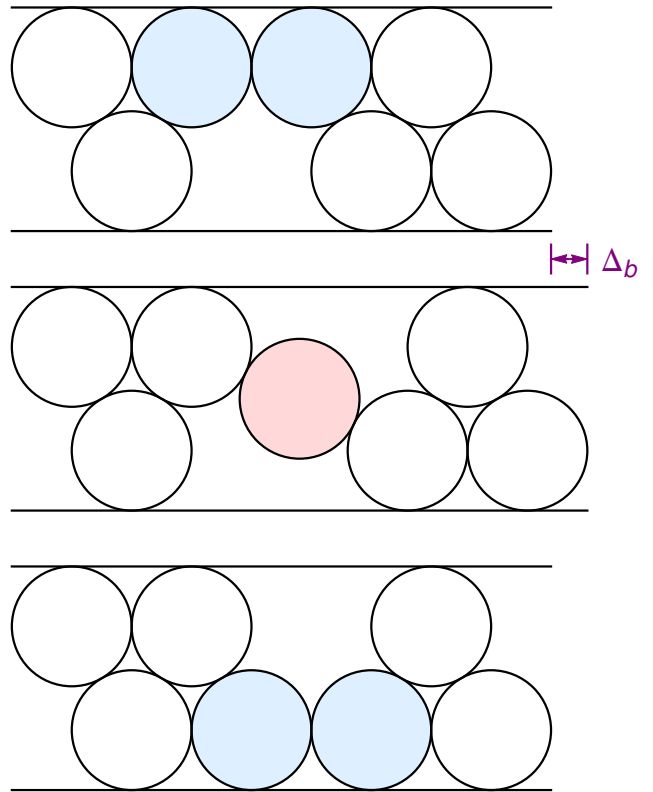


FIG. 7: (Color online) The transition state for motion of a defect. In the top diagram, the two blue-shaded disks are a defect in the zigzag arrangement of disks. The defect can move when one disk crosses the channel by squeezing between its neighbors: the system passes through the transition state shown in the middle diagram to reach the defect state shown in the bottom diagram. In the top diagram the defect involves disks 3 and 4; in the bottom diagram the defect involves disks 4 and 5, when the disks are numbered from the left. The net motion of the defect is to the right, and  $\Delta_b$  is the extra length needed to allow this motion.

We begin by calculating the typical time it takes for a defect to hop to its neighboring site. This was studied in Ref. [4] by means of molecular dynamics, but we shall use transition-state theory [20], which works best when the motion is inhibited and the transition rate is small. The transition state is the state through which the system has to squeeze during the course of a transition: Fig. 7 shows the transition state that our system of hard disks must pass through in order for a defect to move. When the dynamics is not dominated by just the transition state, the more general approach of studying the complete landscape as in Ref. [21] might be useful.

At the transition state, the extra length of the system  $\Delta_b$  over the length which just contains the defect is

$$\Delta_b = \sqrt{4\sigma^2 - h^2} - \sigma - \sqrt{\sigma^2 - h^2}. \quad (27)$$

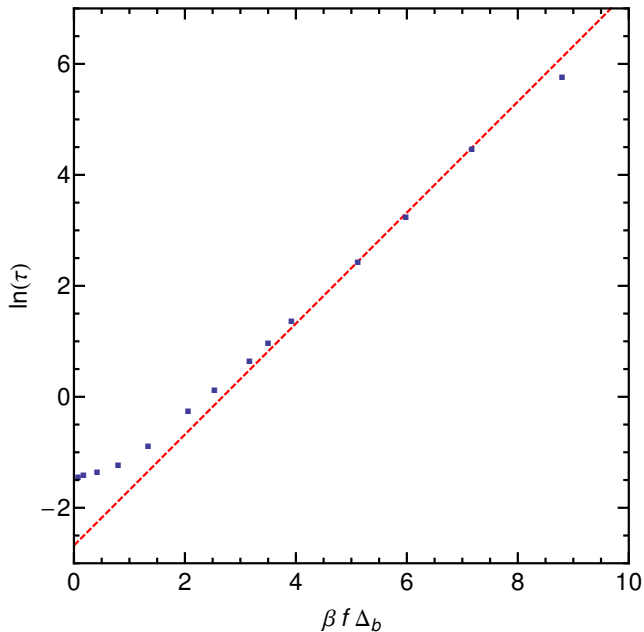


FIG. 8: (Color online)  $\ln(\tau)$ , where  $\tau$  is the time scale on which defects move, plotted against  $\beta f \Delta_b$ .  $\Delta_b$  is defined in Eq. (27) and is the extra length associated with the transition state through which the system must pass to allow a defect to move. The red dashed line is the prediction of our analytical approximation Eq. (28), which would be expected to be exact only for large  $\beta f \Delta_b$ . Data points are from Ref. [4].

The transition rate associated with this saddle is

$$1/\tau = 1/\tau_0 \exp(-\beta f \Delta_b), \quad (28)$$

where  $\tau_0$  is of the order of a disk collision time. In Fig. 8 we have plotted data on  $\tau$  from Ref. [4] as a function of  $\beta f \Delta_b$ . The agreement with (28) is excellent for  $\beta f \Delta_b > 3.5$ , that is for  $\phi > 0.6$ , while at densities closer to  $\phi_d$  the agreement is less satisfactory. But it should be noted that the transition-state approximation is only expected to be good under the same set of circumstances that make our approximations for the equation of state good, that is, for  $\phi \rightarrow \phi_{\max}$ .

We next calculate the transition rate associated with the creation of a pair of defects. (With periodic boundary conditions, as used in Ref. [4], defects can be created only in pairs.) By detailed balance, this rate of creation must equal the rate at which defects move together and annihilate. The transition state for creating a pair of defects is shown in Fig. 9(c). The extra length  $\Delta_c$  required to reach this transition state is

$$\Delta_c = \sqrt{4\sigma^2 - h^2} + \sigma - 3\sqrt{\sigma^2 - h^2}. \quad (29)$$

The transition rate for nucleating two defects or for the rate at which pairs of defects annihilate is then

$$1/\tau_D = 1/\tau_0 \exp(-\beta f \Delta_c). \quad (30)$$

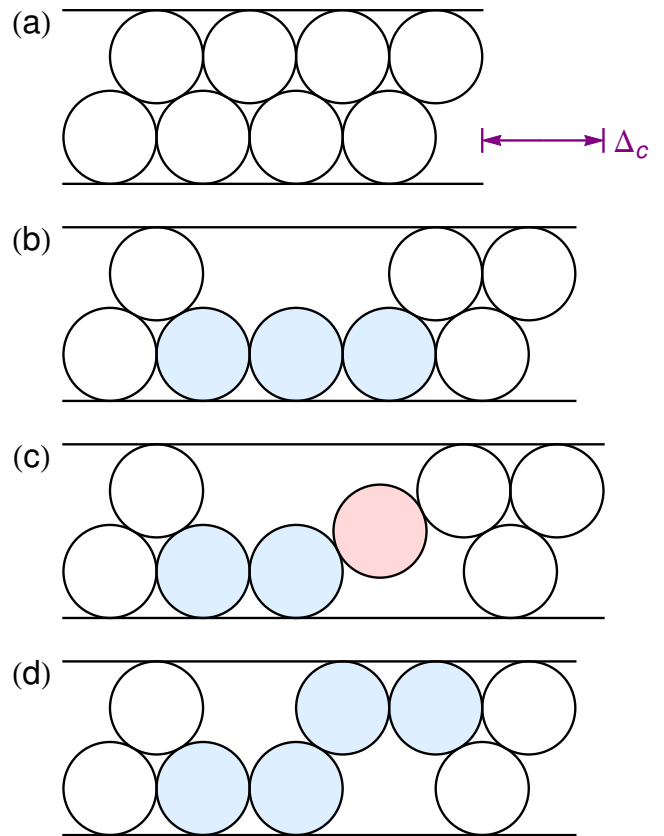


FIG. 9: (Color online) The creation of a pair of defects, starting from the most densely packed state (a). The intermediate state shown in (b) is unstable, as the middle of the three disks in a line can escape upwards. Squeezing through the transition state shown in (c) leads to the two-defect state of (d).  $\Delta_c$  is the extra length occupied by the transition state.

The motion of the defects towards each other so that they might annihilate is probably diffusive. They typically have to diffuse a distance of the order of their spacing  $\xi$  to meet, so that one might expect that

$$\tau_D/\tau \sim \xi^2, \quad (31)$$

where  $\tau$  is the time scale for a defect to hop to a neighboring site by the process illustrated in Fig. 7. Our results for  $\xi$ ,  $\tau$  and  $\tau_D$ , are consistent with Eq. (31). Note that this implies that the diffusion coefficient for defects varies as  $1/\tau$ .

Unfortunately there seem to be no direct studies of  $\tau_D$  in the molecular dynamics literature. We can, however, use our expression for  $\tau_D$  to understand the results of the simulations described in Ref. [3].

In this paper, the authors applied the Lubachevsky–Stillinger (LS) algorithm [5] in which the diameter of the disks was increased at a rate  $\gamma = \sigma^{-1} d\sigma/dt$  in the course of a molecular dynamics simulation starting from a small initial value of  $\sigma$ . They kept the ratio  $H_d/\sigma$

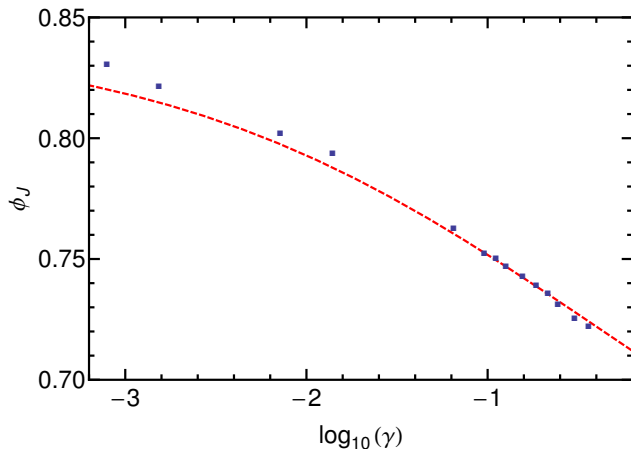


FIG. 10: (Color online) The jammed-state packing fraction  $\phi_J$  plotted against  $\log_{10}(\gamma)$ , where  $\gamma$  is the quench rate. The data points are taken from Ref. [3]. The red dashed line is our prediction of  $\phi_J(\gamma)$  from the Kibble–Zurek mechanism: see the discussion following Eq. (32).

fixed and investigated the  $\gamma$ -dependence of the jammed packing fraction  $\phi_J$ . Their results for  $\phi_J(\gamma)$  (shown in Fig. 10) indicate that  $\phi_J$  is a decreasing function of  $\gamma$ . To understand this, it should first be noted that jammed states with smaller values of  $\phi_J$  contain more defects, the relationship being [2]

$$\begin{aligned} \phi_J &= \frac{N\pi\sigma^2}{4H_d[M\sigma + (N-M)\sqrt{\sigma^2 - h^2}]} \\ &= \frac{\pi\sigma^2}{4H_d[\theta\sigma + (1-\theta)\sqrt{\sigma^2 - h^2}]}. \end{aligned} \quad (32)$$

The hypothesis we shall make, following the ideas of Kibble [6] and Zurek [7], is that when the rate of compression  $\gamma$  exceeds the rate at which defects can annihilate  $1/\tau_D$ , the defect density  $\theta$  is frozen in and is not changed in the last stages of the LS procedure. Thus by equating  $1/\tau_D$  to  $\gamma$  we get an estimate of  $\beta f$  from Eq. (30). This in turn can be used in Eq. (18) to obtain  $\theta$ , which then leads via Eq. (32) to  $\phi_J$ . These estimates of  $\phi_J$  as a function of  $\gamma$  are plotted in Fig. 10, together with the simulational data of Ref. [3]; there is reasonably good agreement between the two.

Eq. (32) also shows that  $\phi_J$  can be regarded as a function of  $\phi$ , which we shall call  $\phi_J(\phi)$ , via the dependence of  $\theta$  on the equilibrium value of  $\phi$ . We can use  $\phi_J(\phi)$  to rewrite Eq. (20) as

$$\beta f = \frac{2N}{L[1 - \phi/\phi_J(\phi)]}. \quad (33)$$

Eq. (28) expresses a relaxation time  $\tau$  in terms of  $\beta f$  and so provides, in conjunction with Eq. (33), an illustration of the Stillinger map idea that was used in Ref. [20] to

explain the relaxation times of systems of hard disks and hard spheres. The Stillinger map of a configuration at packing fraction  $\phi$  is its nearest inherent (jammed) state, with packing fraction  $\phi_J(\phi)$ . In the narrow-channel system, the nearest jammed state is what is obtained in an extremely rapid compression [3]. Notice that for this system  $\beta f$  (and hence  $\tau$ ) diverges only at  $\phi = \phi_{\max}$ : it is only at  $\phi = \phi_{\max}$  that  $\phi = \phi_J(\phi)$ .

## V. POINT-TO-SET LENGTH

In recent years it has been argued that the point-to-set length scale  $\xi_{PS}$  is an important length scale in glasses [22, 23]. It is determined in, say, three dimensions by first equilibrating the system of particles and then freezing all those lying outside a spherical cavity of radius  $R$ . One then studies the correlation function  $C(t) = \langle n(t)n(0) \rangle$  as  $t \rightarrow \infty$ , where  $n$  is the number of particles in a small box at the center of the sphere. If the cavity radius  $R$  is greater than  $\xi_{PS}$ , then  $C(t)$  decays to the value it would have if the particles moved randomly over the volume of the cavity. However, when  $\xi_{PS} > R$  this does not happen, and so by varying  $R$  one can estimate  $\xi_{PS}$ . Basically  $\xi_{PS}$  is a measure of the size of the smallest cavity for which the particles can escape their initial positions when the particles on the boundary are frozen.

In our narrow-channel system we can mimic this procedure by simply freezing all but  $P$  disks, with the  $P$  disks all adjacent to each other. Because in our system each disk interacts only with its nearest-neighbors, one only needs to fix the two disks at the ends of the region which contains the  $P$  disks in typical configurations drawn from an equilibrium distribution. If the packing fraction is  $\phi$ , then the length of the region will be  $R = P\pi\sigma^2/(4H_d\phi)$ . Provided  $R - P\sqrt{\sigma^2 - h^2} > \Delta_c$ , the ‘‘cavity’’ will be large enough to allow the creation of the defects which are needed to enable the system to relax. This fixes a lower bound on  $P$ . Setting  $\xi_{PS} = P\sqrt{\sigma^2 - h^2}$  gives

$$\xi_{PS} \sim \frac{\Delta_c\phi}{\phi_{\max} - \phi}. \quad (34)$$

Note that  $\xi_{PS}$  grows as a simple power law as  $\phi \rightarrow \phi_{\max}$ , whereas the correlation length  $\xi$  grows exponentially rapidly as  $\phi \rightarrow \phi_{\max}$ , as can be seen from Eqs. (26) and (23). As we have pointed out earlier,  $\xi$  (or rather  $\xi\sqrt{\sigma^2 - h^2}$ ) is also the typical distance between defects. Thus a region of size  $\xi_{PS}$  is unlikely to contain any defects in equilibrium, which justifies the use of the relation  $\xi_{PS} = P\sqrt{\sigma^2 - h^2}$ . It also justifies the use of  $\Delta_c$  (rather than  $\Delta_b$ ) as the additional length needed for relaxation, as there will be no defects present to disrupt the zigzag order by their motion.

Activated dynamics is associated with the point-to-set length via

$$\tau = \tau_0 \exp[(\xi_{PS}/l)^\psi], \quad (35)$$

where  $l$  is a length scale of order  $\sigma$ . For agreement with the expressions for, say,  $\tau_D$  or the  $\tau$  of Eq. (28), we would require the exponent to be  $\psi = 1$ .

The two length scales  $\xi$  and  $\xi_{PS}$  relate to different phenomena. In the glass literature  $\xi_{PS}$  is popular [22, 23], as it does not require the identification of the growing structural features which must be behind the onset of caging. In three dimensions, identifying the important clusters is difficult and they may be dependent on details of the interatomic potentials [18, 19]. But a full treatment of glass behavior without such an understanding may be impossible.

## VI. DISCUSSION

All of the equilibrium properties of the model of hard disks in a channel can in principle be determined from the transfer matrix integral equation, but solutions of this equation can only be obtained numerically. One of the purposes of our paper was to show the utility of the analytical approximations which can be found for the limit when  $\phi \rightarrow \phi_{\max}$ . In the same limit, the dynamics of the system is essentially that of a dilute gas of defects. We have discussed some of its basic features, such as the time scales for the creation and annihilation of defects and their diffusion rate.

As is often the case with exactly soluble models, it is hard to calculate some particular quantities. For example, the structure factor  $S(q_x, q_y)$  is the natural function to study for discussing the growth of (say) zigzag order, but we do not know how to obtain it. The dynamics of the model is non-trivial, and here much remains to be done, via simulations and analytical approaches. We have in mind here the study and understanding of the autocorrelation function of Eq. (10).

One of the pleasing features of this model is that it has features that mimic the behavior of three-dimensional spheres at the packing fraction  $\phi \simeq 0.58$ ; that is, it has an avoided dynamical transition at  $\phi_d$ . Above this density the dynamics involves cooperative movements of the disks and is activated. Approach to  $\phi_d$  from lower densities is accompanied by the growth of the length scale  $\xi$  and when this is large enough, caging appears. We suspect that such a feature might be present in higher dimensions, but the growth of the cage may require study of more subtle correlations than those captured by the structure factor, for example those studied in Ref. [18].

## Acknowledgments

We should like to thank Richard Bowles and Mahdi Zaeifi Yamchi for sharing their data and insights.

- 
- [1] A. J. Liu and S. R. Nagel, *Nature (London)*, **396**, 21, (1998).
  - [2] M. Z. Yamchi, S. S. Ashwin, and R. K. Bowles, *Phys. Rev. Lett.* **109**, 225701 (2012)
  - [3] S. S. Ashwin, M. Zaeifi Yamchi, and R. K. Bowles, *Phys. Rev. Lett.* **110**, 145701 (2013).
  - [4] R. K. Bowles and I. Saika-Voivod, *Phys. Rev. E* **73**, 011503 (2006).
  - [5] B. D. Lubachevsky and F. H. Stillinger, *J. Stat. Phys.* **60**, 561 (1990).
  - [6] T. W. B. Kibble, *J. Phys. A* **9**, 1397 (1976).
  - [7] W. H. Zurek, *Nature (London)* **317**, 505 (1985).
  - [8] D. A. Kofke and A. J. Post, *J. Chem. Phys.* **98**, 4853 (1993).
  - [9] L. Tonks, *Phys. Rev.* **50**, 955 (1936).
  - [10] M. J. Godfrey and M. A. Moore, to be published.
  - [11] E. P. Bernard and W. Krauth, *Phys. Rev. Lett.* **107**, 155704 (2011).
  - [12] W. Kob, S. Roldán-Vargas, and L. Berthier, *Nature Physics* **8**, 164 (2012).
  - [13] M. J. Godfrey and M. A. Moore, unpublished.
  - [14] A. S. Keys, A. R. Abate, S. C. Glotzer, and D. J. Durian, *Nature Physics* **3**, 260 (2007).
  - [15] T. Narumi, S. V. Franklin, K. W. Desmond, M. Tokuyama, and E. R. Weeks, *Soft Matter* **7**, 1472 (2011).
  - [16] G. Brambilla, D. El Masri, M. Pierno, L. Berthier, L. Cipelletti, G. Petekidis, and A. B. Schofield, *Phys. Rev. Lett.*, **102**, 085703 (2009).
  - [17] Z. W. Salsburg and W. W. Wood, *J. Chem. Phys.* **37**, 798 (1962).
  - [18] A. Malins, J. Eggers, H. Tanaka, and C. P. Royall, *Faraday Discuss.* **167**, 405 (2013).
  - [19] M. Leomach and H. Tanaka, *Nature Communications* **3**, 974 (2012).
  - [20] M. Barnett-Jones, P. A. Dickinson, M. J. Godfrey, T. Grundy, and M. A. Moore, *Phys. Rev. E* **88**, 052132 (2013).
  - [21] G. L. Hunter and E. R. Weeks, *Phys. Rev. E* **85**, 031504 (2012).
  - [22] C. Cammarota, A. Cavagna, G. Gradenigo, T. S. Grigera and P. Verrocchio, *J. Chem. Phys.* **131**, 194901 (2009); *J. Stat. Mech.* L12002 (2009).
  - [23] A. Cavagna, T. S. Grigera, and P. Verrocchio, *J. Chem. Phys.* **136**, 204502 (2012).